

FSTL3 deletion reveals roles for TGF- β family ligands in glucose and fat homeostasis in adults

Abir Mukherjee*, Yisrael Sidis*, Amy Mahan*, Michael J. Raher¹, Yin Xia*, Evan D. Rosen², Kenneth D. Bloch³, Melissa K. Thomas⁵, and Alan L. Schneyer¹¶

*Reproductive Endocrine Unit, ¹Division of Cardiology, and ²Laboratory of Molecular Endocrinology and Diabetes Unit, Massachusetts General Hospital, Boston, MA 02114; and ³Division of Endocrinology, Diabetes, and Metabolism, Beth Israel Deaconess Medical Center, Boston, MA 02215

Edited by Patricia K. Donahoe, Massachusetts General Hospital, Boston, MA, and approved November 27, 2006 (received for review September 11, 2006)

Activin and myostatin are related members of the TGF- β growth factor superfamily. FSTL3 (Follistatin-like 3) is an activin and myostatin antagonist whose physiological role in adults remains to be determined. We found that homozygous FSTL3 knockout adults developed a distinct group of metabolic phenotypes, including increased pancreatic islet number and size, β cell hyperplasia, decreased visceral fat mass, improved glucose tolerance, and enhanced insulin sensitivity, changes that might benefit obese, insulin-resistant patients. The mice also developed hepatic steatosis and mild hypertension but exhibited no alteration of muscle or body weight. This combination of phenotypes appears to arise from increased activin and myostatin bioactivity in specific tissues resulting from the absence of the FSTL3 antagonist. Thus, the enlarged islets and β cell number likely result from increased activin action. Reduced visceral fat is consistent with a role for increased myostatin action in regulating fat deposition, which, in turn, may be partly responsible for the enhanced glucose tolerance and insulin sensitivity. Our results demonstrate that FSTL3 regulation of activin and myostatin is critical for normal adult metabolic homeostasis, suggesting that pharmacological manipulation of FSTL3 activity might simultaneously reduce visceral adiposity, increase β cell mass, and improve insulin sensitivity.

activin | diabetes | metabolism | myostatin | β cell

Members of the TGF- β superfamily of growth factors play diverse roles in embryonic development as well as in organ homeostasis and injury/pathogen response in adults (1). Activin and myostatin form one structurally related branch of the TGF- β family that utilizes common cell-surface receptors and Smad second messengers (2–4). Activin is a critical regulator of embryonic cell fate determination and organ development as well as adult organ homeostasis (5). Activin deletion in mice results in developmental defects and early neonatal death (6), whereas activin overexpression results in cancer, cachexia, and liver necrosis (3, 7, 8). Loss of myostatin expression results in increased muscle mass and reduced adiposity (9–11), whereas overexpression of myostatin leads to a severe reduction of both muscle and adipose tissue mass, along with cachexia (12, 13). These findings demonstrate the requirement for tight regulation of activin and myostatin activity to maintain normal adult physiology.

Regulation of activin and myostatin activity occurs at multiple levels. Among the extracellular regulators, FSTL3 (follistatin-like-3) and FST (follistatin) are structurally and functionally related glycoproteins that bind and antagonize actions of both activin and myostatin (14, 15). FSTL3 expression is highest in placenta, followed by testis, pancreas, and heart, whereas FST expression is high in ovary, testis, and kidney, suggesting that they may have nonoverlapping actions in different organs (16). Circulating FST was largely bound to activin (17), whereas FSTL3 was isolated from human and mouse serum as a complex with myostatin (18), indicating that FSTL3 and FST may be important physiological regulators of circulating myostatin and activin.

One experimental approach to examine the importance of regulating activin and myostatin action is to inactivate their physiological antagonists. Deletion of *Fst* resulted in a number of developmental defects and early neonatal death, confirming the importance of FST in mammalian development (19), although the early neonatal death precluded determination of the physiological roles of FST in juveniles and adults. Recently, *FST* was deleted specifically in adult ovaries which resulted in premature cessation of ovarian activity (20), confirming that FST indeed has important roles in postpubertal gonadal function in adults.

To determine the physiological actions of FSTL3, we generated *Fstl3*-null mice. In contrast to *Fst*-null mice, *Fstl3*-deficient animals survive to adulthood and develop a suite of metabolic phenotypes that collectively suggest that FSTL3 and the activin and myostatin ligands it regulates have important metabolic roles in the adult that were heretofore underappreciated.

Results

Generation of FSTL3 Knockout (KO) Mice. We generated mice heterozygous for an *Fstl3* allele missing exon 1 [see supporting information (SI) Fig. 6A and B] that, when mated, produced homozygote *Fstl3*^{tm1Alc} (FSTL3 KO) mice in expected Mendelian ratios that survived to adulthood, allowing analysis of the effect of global FSTL3 deletion in adult mice. Although FSTL3 mRNA was detectable in WT heart, testis, white fat, and muscle, it was undetectable in KO mice (SI Fig. 6C and D), verifying that FSTL3 was no longer expressed.

No Change in Body Weight or Muscle Composition in FSTL3 KO Mice. Because myostatin overexpression results in reduced muscle and fat mass (13) and FSTL3 deletion should increase myostatin bioactivity due to its identification as a circulating myostatin binding protein (18), we analyzed age-related changes in body weight in FSTL3 KO mice. The distribution of age-specific body weights in 1- to 4-month-old mice was not different between genotypes (Fig. 1A), nor were the mean body weights of 6- to 12-month-old mice (Fig. 1B). Moreover, there was no detectable difference between FSTL3 KO and WT mice in gastrocnemius and quadriceps muscle weight (Fig. 1C) or histological appearance (see SI Fig. 7A and B), and analysis

Author contributions: A. Mukherjee, Y.S., Y.X., E.D.R., K.D.B., M.K.T., and A.L.S. designed research; A. Mukherjee, Y.S., A. Mahan, M.J.R., Y.X., and A.L.S. performed research; M.J.R., K.D.B., and M.K.T. contributed new reagents/analytic tools; A. Mukherjee, Y.S., A. Mahan, M.J.R., Y.X., E.D.R., K.D.B., M.K.T., and A.L.S. analyzed data; and A. Mukherjee, M.J.R., K.D.B., M.K.T., and A.L.S. wrote the paper.

The authors declare no conflict of interest.

This article is a PNAS direct submission.

Abbreviations: KO, knockout; PEPCCK, phosphoenolpyruvate carboxykinase; G6Pase, glucose-6-phosphatase.

¶To whom correspondence should be addressed at: Reproductive Endocrine Unit, BHX-5, Massachusetts General Hospital, 55 Fruit Street, Boston, MA 02114. E-mail: schneyer.alan@mgh.harvard.edu.

This article contains supporting information online at www.pnas.org/cgi/supplemental.

© 2007 by The National Academy of Sciences of the USA

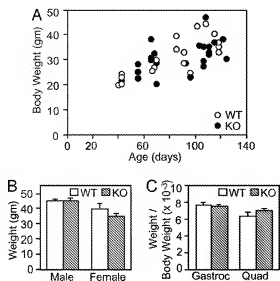


Fig. 1. Growth rate and body weights of FSTL3 KO and WT mice. (A) Distribution of age versus body weight of WT and FSTL3 KO male mice is shown for 1- to 4-month-old animals. (B) Mean body weights of male (average age, 9 months; $n = 20$ WT and 34 KO) and female (average age, 11 months; $n = 11$ WT and 27 KO) WT and KO mice. (C) Weights of dissected quadriceps (Quad) and gastrocnemius (Gastroc) muscles expressed as a ratio to body weight ($n = 25$ WT and 58 KO).

of muscle fiber area distribution of five WT and five KO animals revealed no significant differences (see SI Fig. 7C). These results indicate that loss of FSTL3 did not produce a detectable decrease in body weight, muscle mass, or fiber area, as might be expected if myostatin bioactivity were elevated with the loss of a circulating antagonist.

Increased Pancreatic Islet Size in FSTL3 KO Animals. Previous studies have suggested that activin regulates pancreatic β cell proliferation, islet size, and glucose-stimulated insulin secretion (21–23). Because FSTL3 is highly expressed in the pancreas (16), we examined the effect of FSTL3 deletion on pancreatic islets. Representative pancreas sections at low magnification from WT and FSTL3 KO mice immunocytochemically stained for insulin (Fig. 2*A* and *B*, respectively) demonstrate that FSTL3 KO islets are substantially larger than those from WT littermates. At higher magnification, the presence of more intra-islet capillaries can be discerned in FSTL3 KO islets (Fig. 2*D*) compared with WT islets (Fig. 2*C*). Immunofluorescence analysis demonstrated that these larger FSTL3 KO islets contained more insulin-expressing β cells (Fig. 2*F*) compared with WT islets (Fig. 2*E*). In addition, although α cells were readily identified at the periphery of WT islets (Fig. 2*E*, white arrows), very few were found in the periphery of KO islets, whereas the majority of green staining resulted from nonspecific fluorescence from red blood cells within KO islets (Fig. 2*F*). Morphometric analysis of 36 WT and 99 KO islets revealed that mean islet size was nearly 50% larger in FSTL3 KO mice (Fig. 2*G*), but β cell size was not different (Fig. 2*H*), indicating that larger islets resulted from β cell hyperplasia. Moreover, FSTL3 KO mice had a broader distribution of islet sizes, with the islet size group containing the most islets being smaller than that for WT islets. In addition, FSTL3 KO islets contained a distinct population much larger than any observed in WT mice (Fig. 2*I*). This distribution increased the number of islets observed per section (Fig. 2*I* *Inset*). Taken together, these analyses suggest that existing islets grew larger because of β cell hyperplasia in FSTL3 KO mice although there was also a likely increase in islet neogenesis, all

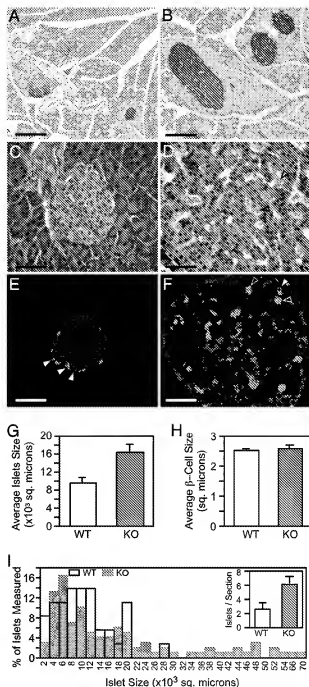


Fig. 2. Increased pancreatic islet size in FSTL3 KO mice. (A and B) Low-power photomicrographs of WT (A) and FSTL3 KO (B) pancreas immunocytochemically stained for insulin. (C and D) H&E staining of the same WT (C) and KO (D) tissues. Black arrowheads show numerous capillaries within the KO islet. (E and F) Immunofluorescence photographs showing insulin (red) and glucagon (green) localization in islets from WT (E) and KO (F) mice. In the KO islets, the majority of green staining is nonspecific staining of red blood cells within the islet, shown by open arrowheads. Glucagon-producing α cells in both WT and KO islets are shown by solid arrowheads. (Magnifications: A and B, $\times 5$; C–F, $\times 40$) (Scale bars, A and B, 200 μ m; C–F, 50 μ m). (G–I) Histomorphometric analyses of pancreatic islets. Average islet size (G) ($n = 36$ WT and 99 KO) and β cell size (H) ($n = 119$ WT and 94 KO) in pancreas from WT and KO animals ($n = 6$ WT and 8 KO) (values shown in squared micrometers). (I) Size distribution of pancreatic islets in WT and KO animals, percent of total number of islets counted is plotted against islet size. (Inset) The mean number of islets seen per section of WT and KO animals. Both islets per section and average islet size is significantly increased ($P < 0.05$) in KO pancreas. All error bars are SEM.

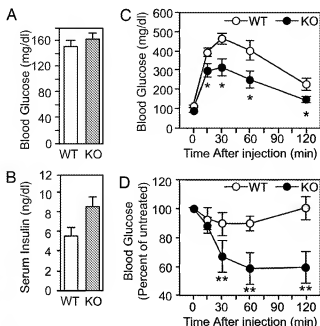


Fig. 3. Enhanced glucose metabolism in FSTL3 KO mice. (A) Glucose levels in tail blood of random-fed WT and KO mice are not different ($n = 17$ WT and 30 KO). (B) Serum insulin levels in these same mice are significantly greater ($P < 0.05$) in KO animals compared with WT littermates. (C) Glucose tolerance test showing mean glucose levels of five animals per group after i.p. injection of 2 g/kg glucose at time 0. *, $P < 0.05$. (D) Insulin tolerance test showing glucose levels as a ratio to untreated glucose concentration (at time -15 min). Insulin (1 unit/kg) was injected i.p. at time 0. Glucose levels were significantly lower in FSTL3 KO mice from 30–120 min. **, $P < 0.01$. A total of 24 WT and KO mice were examined in these studies. All error bars are SEM.

of which may be due to increased activin bioactivity resulting from loss of FSTL3.

Altered Glucose Homeostasis in FSTL3 KO Animals. We next examined whether the larger and more numerous islets altered glucose homeostasis in FSTL3 KO mice. In 9-month-old, random-fed animals, there was no significant difference in serum glucose levels between FSTL3 KO mice and WT littermates (Fig. 3A). However, insulin concentrations were significantly ($P < 0.05$) elevated in these same mice (Fig. 3B), suggesting that they might be insulin-resistant. To examine the dynamic response to glucose and insulin, we performed glucose and insulin tolerance tests. FSTL3 deletion significantly enhanced both glucose tolerance (Fig. 3C; $P < 0.05$) and insulin sensitivity (Fig. 3D; $P < 0.01$) in FSTL3 KO mice relative to WT littermates, indicating that the islets in FSTL3 KO mice were not enlarged secondary to insulin resistance. These alterations in glucose and insulin homeostasis, along with the enlarged islets and increased β cell mass in FSTL3 KO mice, are consistent with FSTL3 regulation of activin bioactivity being critical for normal control of glucose metabolism in the adult.

Alterations in Liver Function in FSTL3 KO Mice. Because the liver is a major regulator of glucose metabolism (24) and activin may play a role in liver homeostasis (25, 26), we next determined whether FSTL3 deletion altered hepatic structure and function. Hepatic steatosis was detectable at 5 months of age in FSTL3 KO animals but not in WT littermates (data not shown) and increased in severity by 9 months (Fig. 4A–D). Oil Red O staining confirmed extensive macrovesicular and microvesicular steatosis in FSTL3 KO mice (Fig. 4F) that was absent in WT littermates (Fig. 4E). However, there were no significant differences be-

tween FSTL3 KO and WT littermates in circulating free fatty acid or triglyceride concentrations (see SI Table 1). Moreover, there was no evidence of hepatic necrosis or fibrosis. In addition, serum concentrations of amino aspartate and amino alanine transferase enzymes, indicators of hepatocyte distress (27), were not different between the genotypes (see SI Table 1). These data indicate that overall liver function was not compromised in FSTL3 KO mice.

To further address the liver's role in the altered glucose dynamics in FSTL3 KO mice, we examined liver glycogen stores and found that glycogen content was substantially reduced in FSTL3 KO livers (Fig. 4H) compared with WT littermates (Fig. 4G). In addition, quantitative PCR analyses revealed that expression of key gluconeogenic enzymes phosphoenolpyruvate carboxykinase (PEPCK) and glucose-6-phosphatase (G6Pase) was elevated by 6- and 4.5-fold, respectively, in FSTL3 KO livers compared with WT littermates (Fig. 4I), indicating that gluconeogenesis was elevated in FSTL3 KO mice. We next evaluated whether activin or myostatin could directly regulate PEPCK or G6Pase mRNA expression by using HepG2 hepatoma cells. Activin treatment significantly increased G6Pase expression 1.3-fold ($P < 0.05$), whereas myostatin treatment suppressed G6Pase expression $>50\%$ ($P < 0.01$) (Fig. 4J), indicating that activin can directly enhance G6Pase mRNA expression. Thus, up-regulated gluconeogenesis in FSTL3 KO mice may be partially due to direct actions of activin on hepatocyte gene expression as well as a homeostatic response to prevent hypoglycemia due to mild, chronic hyperinsulinemia arising from the enlarged islets.

Alterations in Fat Deposition in FSTL3 KO Mice. Because myostatin overexpression also reduced fat mass (13), we examined adipose tissues in FSTL3 KO animals. Both male and female FSTL3 KO mice had significantly smaller abdominal visceral fat depots compared with WT littermates (Fig. 5A and B, respectively). However, the fraction of body weight estimated to be composed of fat was not different between genotypes (Fig. 5C). Histological (see SI Fig. 8A and B) and histomorphometric (see SI Fig. 8C) analyses demonstrated that the adipocyte size distribution in FSTL3 KO mice was not different from that in WT littermates, suggesting that the reduced fat pad weights were due to fewer adipocytes in FSTL3 KO mice. Despite the reduced abdominal fat pad mass in FSTL3 KO animals, serum concentrations of leptin and adiponectin, two adipokines that typically reflect fat mass, were not significantly altered (see SI Table 1). Taken together, these results suggest that fat storage is preferentially shifted from visceral to s.c. depots and/or other organs in FSTL3 KO mice. Because previous studies have demonstrated that myostatin administration at low, subpharmacological levels reduced only visceral fat mass (13) and not muscle mass, it is likely that increased myostatin bioactivity resulting from deletion of FSTL3 resulted in altered visceral fat deposition.

FSTL3 KO Animals Are Hypertensive. Because FSTL3 is highly expressed in heart tissue (16), we examined weight and function of hearts in 9-month-old female FSTL3 KO mice. We found that heart weight relative to body weight, left ventricular end systolic pressure, and systolic arterial pressure were all significantly increased compared with WT littermates (see SI Fig. 9A–C). These observations demonstrate that mice lacking FSTL3 have altered cardiac structure and function that results in hypertension by 9 months of age.

Discussion

The activity of TGF- β superfamily growth factors is regulated at multiple levels. Regulators such as FSTL3 and FST constitute a subfamily of follistatin domain proteins that bind and neutralize TGF- β family ligands, including activin and myostatin (14). The

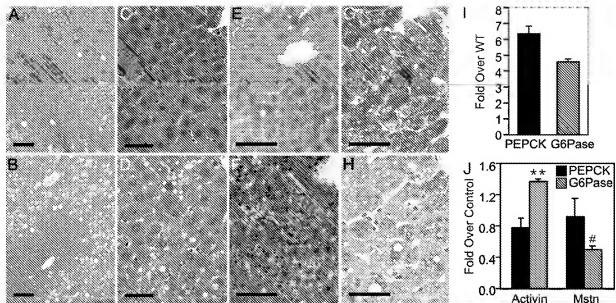


Fig. 4. Liver phenotypes of FSTL3 KO mice. (A–D) H&E staining of livers from WT (A and C) and KO (B and D) animals. (E and F) Frozen sections of liver stained with Oil Red O from WT (E) and KO (F) animals at 9.5 months. (G and H) Liver sections stained with Periodic acid-Schiff's stain showing vastly reduced glycogen content in FSTL3 KO mice (H) compared with WT littermates (G). (Magnifications: A and B, $\times 10$; C–H, $\times 40$.) (Scale bars, A and B, 100 μ m; C–H, 50 μ m.) (I) Gluconeogenic genes PECK and G6Pase are significantly ($P < 0.05$) elevated in FSTL3 KO mice relative to WT mice by 6- and 4.5-fold, respectively, as analyzed by quantitative PCR. (J) Activin (5 ng/ml) significantly ($P < 0.01$) stimulated G6Pase gene expression relative to untreated HepG2 liver hepatoma cells, whereas myostatin (25 ng/ml) suppressed G6Pase under the same conditions ($P < 0.05$).

critical importance of this regulation is emphasized by the previously described defects and early neonatal death resulting from *Fst* deletion (19). We now report that, in contrast to *Fst*-null mice, *Fstl3*-null mice survive to adulthood and are fertile, permitting investigation of the role of a natural activin and myostatin antagonist in adults. By 9 months of age, these mice developed a number of metabolic phenotypes, including increased pancreatic β cell mass and islet number, reduced visceral fat mass, elevated postprandial insulin concentrations, reduced hepatic glycogen, up-regulated gluconeogenesis, hepatic steatosis, and hypertension. These phenotypes were not secondary to peripheral insulin resistance because FSTL3 KO mice were more glucose-tolerant and insulin-sensitive than WT littermates. These findings demonstrate that FSTL3 has important roles in adult physiology, the abrogation of which results in altered glucose and lipid homeostasis. Because FSTL3 is an activin and myostatin antagonist (14), these phenotypes further imply that activin and/or myostatin have critical roles in regulating metabolism that were previously unappreciated.

FSTL3 KO mice have enlarged and more numerous pancreatic islets that primarily contain β cells, suggesting that FSTL3

influences islet size through altering β cell proliferation, survival, and/or differentiation. Activin mRNA, protein, and receptors have been detected previously in β cells (28, 29), and activin treatment increased β cell proliferation (23) and glucose-stimulated insulin secretion in rat and human islet cultures (21, 30). Moreover, transgenic mice expressing a dominant-negative activin receptor in islets had reduced β cell mass (31). In light of these findings, our observations suggest that FSTL3 deficiency resulted in augmented activin bioactivity within islets that induced increased β cell mass, islet size, and islet number *in vivo*. Moreover, enhanced glucose-stimulated insulin production resulting from this increased activin action in β cells could be at least partially responsible for the elevated postprandial insulin concentrations observed in FSTL3 KO mice.

The number and size of islets and the β cells they contain can vary in response to changing metabolic demands (32). Potential sources for these new islets and β cells include β cell proliferation (33) and/or recruitment from progenitor/stem cells (34). Activin has been reported to accelerate proliferation of β cells (23) but also to promote differentiation of ductal cells (35), suggesting that loss of FSTL3 and the consequent increase in activin activity leads to increased β cell proliferation and recruitment that together result in the larger β cell mass and the biphasic distribution of islet size we observed in FSTL3 KO mice.

Because pharmacological overexpression of myostatin in adults decreased muscle mass, visceral fat deposition, and development of cachexia (13) and because circulating myostatin was found complexed with FSTL3 (18), we hypothesized that FSTL3 KO mice would develop decreased total body weight and muscle mass with age. However, we were unable to detect any difference in growth patterns, muscle mass, or muscle fiber size between the genotypes. Importantly, it has been shown that administration of smaller (e.g., 1 μ g) doses of myostatin resulted in nearly 50% reduction of visceral fat mass with no changes in body weight, muscle weight, or muscle diameter (13), suggesting that visceral adipose is more sensitive to myostatin action than muscle mass in adults. Because the total body fat of FSTL3 KO

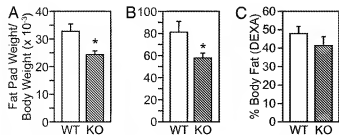


Fig. 5. Fat depot mass is reduced in FSTL3 KO mice. (A and B) Reduced visceral abdominal fat pad mass in FSTL3 KO males (A) ($n = 25$ WT and 56 KO, $P = 0.005$) and females (B) ($n = 19$ WT and 42 KO, $P < 0.05$). (C) Percent body fat of WT and FSTL3 KO mice, as measured by dual emission x-ray absorptiometry ($n = 6$ WT and 7 KO). All error bars are SEM.

mice was not significantly different from WT littermates but visceral fat was significantly reduced, increased myostatin bioactivity resulting from FSTL3 deletion may redirect lipid deposition from visceral fat pads to s.c. fat depots or to other tissues that are not myostatin-responsive. Thus, the reduced visceral fat mass observed in FSTL3 KO mice may be a primary action of excess myostatin bioactivity resulting from loss of its antagonist. Because accumulation of visceral fat is associated with glucose intolerance and insulin resistance (36), this myostatin-dependent reduction of visceral fat in FSTL3 KO mice may be responsible, at least in part, for the enhanced glucose tolerance and insulin sensitivity in FSTL3 KO mice. It is also possible that the improved glucose tolerance derives to some extent from direct actions of myostatin and/or activin on adipocytes (or muscle) to increase insulin-stimulated glucose uptake.

We propose that the phenotype of the FSTL3 KO mouse derives from loss of FSTL3 regulation of activin and myostatin in multiple tissues. One possibility is that mild, chronic hyperinsulinemia resulting from the increased β cell mass promotes glucose uptake by muscle, fat, and other tissues, which could be potentiated acutely by an activin-mediated increase in glucose-stimulated insulin secretion (21). To avoid hypoglycemia, FSTL3 KO mice would have a chronic need for generating glucose, thereby accounting for the vastly up-regulated gluconeogenic gene expression and decreased glycogen content observed in FSTL3 KO livers. However, because insulin normally suppresses gluconeogenesis through down-regulation of gluconeogenic enzyme expression (37), the enhanced gluconeogenesis might indicate that FSTL3 KO hepatocytes are mildly resistant to insulin. Alternatively, because we found that activin stimulated G6Pase mRNA expression in HepG2 hepatoma cells, the elevated gluconeogenic enzyme mRNA expression in FSTL3 livers could derive, at least in part, from the direct action of activin on hepatocytes, which exceeds the inhibition from insulin. Finally, the reduction in visceral fat mass in FSTL3 KO mice may lead to enhanced insulin sensitivity given that reductions in visceral fat mass are associated with improved insulin sensitivity (36).

Our results demonstrate that FSTL3 deletion, along with the presumed tissue-selective increase in activin and myostatin activity, has significant actions in regulating glucose homeostasis and lipid distribution. Pharmacologic interventions to promote human characteristics that resemble those in the FSTL3 KO mouse, including reduced visceral adiposity, enhanced insulin sensitivity, and augmentation of endogenous insulin production and β cell mass and function, could be potentially beneficial for the treatment of metabolic disorders, such as obesity, metabolic syndrome, and diabetes. Because the phenotypes were caused by deletion of a circulating binding protein, our results further suggest that development of FSTL3 antagonists or activin and/or myostatin agonists could present viable approaches for developing therapeutic agents to treat human metabolic disease.

Materials and Methods

Generation of *Fstl3*-Deletion Mouse. The *Fstl3* gene targeting vector was prepared by introducing a loxP sequence downstream of exon 1 at a BspHI site, and a floxed neomycin resistance gene (Neo) was inserted at an XbaI site 1.6 kb upstream of BspHI, thus flanking a 1.6-kb region of the *Fstl3* gene surrounding exon 1 by two loxP sequences. J1 ES cells were transfected, selected for correct *Fstl3* gene targeting, and microinjected into C57BL/6 mice blastocysts. Chimeric male mice were bred with C57BL/6 females, and their agouti pups were genotyped. Animals carrying the *Fstl3* targeted allele were then bred with transgenic *Elia-Cre* mice. *Fstl3*-gene-targeted and Cre-positive animals were bred with WT animals to segregate the various recombinant alleles. Offspring were genotyped to identify Neo excision in animals that had undergone either partial recombination to produce a conditional *Fstl3* allele or a complete recombination to produce an *Fstl3* exon 1 deletion allele.

These latter heterozygous animals were bred to obtain homozygous *Fstl3*-null mice (*Fstl3*^{tm1.1Aloc/tm1.1Aloc}). All animal studies complied with US Department of Agriculture guidelines under an animal-use protocol approved by the Massachusetts General Hospital Subcommittee on Research Animal Care.

DNA Analyses for Genotyping. DNA prepared from ES cells or tail biopsies were analyzed for genotyping either by Southern blot analysis, after appropriate restriction enzyme digestion, or by PCR as previously described in ref. 38 (see *SI Methods* for details).

RNA Analyses: Northern Blot and RT-PCR. Total RNA was extracted from tissues with TRIzol (Invitrogen, Carlsbad, CA). FSTL3 mRNA expression was assessed by Northern blot analysis with 10 μ g of total RNA and a radiolabeled full-length mouse FSTL3 cDNA probe. Alternatively, 1 μ g of total RNA was reverse-transcribed and used in quantitative PCR by using SYBR green incorporation with reagents from Stratagene (La Jolla, CA) on a Stratagene MX4000. A cDNA standard was run in each PCR for each target, and message concentrations were normalized to mouse ribosomal protein 1.19.

HepG2 Hepatoma Cell Culture and Analysis. HepG2 cells cultured in RPMI medium containing 10% FCS and antibiotics for 24–48 h were treated with fresh medium containing either 5 ng/ml activin or 25 ng/ml myostatin (R & D Systems, Minneapolis, MN) for an additional 16 h. Cells were then extracted with TRIzol (Invitrogen, Carlsbad, CA) and analyzed for mRNA expression level by quantitative PCR.

Serum Hormone Measurements. Serum hormone measurements were conducted by specific RIA, ELISA, or biochemical assay in the Reproductive Endocrine Unit Assay Core and the Boston Area Diabetes Endocrinology Research Center RIA Core Laboratory at Massachusetts General Hospital.

Histology and Histomorphometry. Tissues were isolated from mice at different ages and fixed in 4% paraformaldehyde overnight. The tissues were then processed for paraffin embedding. Multiple 6- μ m-thick microtome sections from each tissue were stained with H&E and photographed. For measurement of islet size in pancreas, 20 consecutive 8- μ m sections were H&E-stained and photographed. For each pancreas, all islets in two sections at least 80 μ m apart were counted, and their area measured with SPOT image analyses software. For white adipocyte size measurement, all adipocytes in each field were counted, and the area was measured with ImageJ software. Muscle fiber size was similarly quantitated by using three $\times 40$ fields.

Immunofluorescence and Immunohistochemistry. Immunofluorescence was performed as previously described in ref. 38 (see *SI Methods* for details). The primary antibodies used were either a guinea pig anti-insulin (Linco Research, St. Charles, MO) or a mouse anti-glucagon antibody (Sigma, St. Louis, MO). The secondary antibodies used were anti-mouse-FITC or an anti-guinea pig-TRITC (Jackson ImmunoResearch Laboratories, West Grove, PA). For immunohistochemical detection, the sections were processed with a Vectastain Elite ABC kit (Vector Laboratories, Burlingame, CA) and 3,3'-diaminobenzidine (ICN Biomedicals, Solon, OH) and counterstained. For pancreatic β cell size estimation, 3,3'-diaminobenzidine-stained areas developed after immunohistochemical detection of insulin were measured with SPOT software and divided by the number of blue-stained nuclei counted.

Oil Red O Staining. Freshly dissected liver and muscle were fixed overnight in 4% paraformaldehyde, cryoprotected in 30% sucrose in PBS for another day, and then frozen in OCT blocks. Cryostat sections 10 μ m thick were processed for Oil Red O staining as described in ref. 39 in a 0.3% solution of Oil Red O in 60% isopropanol for 1 h. After being washed, sections were counterstained with Gills hematoxylin.

Determination of Total Body Fat. Body fat content of FSTL3 KO and WT mice was measured by dual emission x-ray absorptiometry with a PIXImus2 Mouse Densitometer (GE Medical Systems, Madison, WI).

Glucose and Insulin Tolerance Tests. For glucose tolerance tests, animals fasted overnight and then were weighed, and their fasting blood glucose levels were measured by using a glucometer (OneTouch Ultra; Lifescan, Milpitas, CA). Mice were injected i.p. with glucose (2 g of D-glucose per kg of body weight), and blood glucose levels were assessed 15, 30, 60, and 120 min after injection. Insulin tolerance tests were performed similarly,

except that animals fasted for 2–3 h and then were injected i.p. with human regular insulin at a concentration of 1 unit of insulin per kg of body weight (Eli Lilly, Indianapolis, IN).

Hemodynamic Analyses. Mice were anesthetized with 100 mg/kg ketamine, 250 μ g/kg fentanyl, and 2 mg/kg pancuronium, intubated, and mechanically ventilated (10 μ l per g of body weight, 120 bpm, $\text{FiO}_2 = 1$). A ventricular catheter (PE-10; Miller Instruments, Houston, TX) was placed for continuous monitoring of the heart rate and blood pressure.

We thank Dr. Ernestina Schipani and Jeffrey Lange for assistance with histology and dual emission x-ray absorptiometry analysis, Dr. Odile Peroni for facilitating dynamic metabolic testing, Dr. Milton Fiedler for providing expert analysis of liver pathology, and Dr. Joseph Avruch for critical evaluation of the manuscript. This work was supported by National Institutes of Health Grant R01HL39777/DK076143 (to A.L.S.) with assistance from Boston Area Diabetes Endocrinology Research Center Grant P30DK57521 and by National Institutes of Health Grant R01HL070896 (to M.J.R. and K.D.B.).

- Shi Y, Massague J (2003) *Cell* 113:685–700.
- Rebbapragada A, Benchabane H, Wraja JL, Celeste AJ, Attisano L (2003) *Mol Cell Biol* 23:7230–7242.
- Lee SJ, Reed LA, Davies MV, Gengenath S, Goad MEP, Tomkinson KN, Wright JF, Barker C, Ehrmantraut G, Holmstrom J, et al. (2005) *Proc Natl Acad Sci USA* 102:18117–18122.
- Welt C, Sidis Y, Keutmann H, Schneyer A (2002) *Exp Biol Med* 227:724–752.
- Jones KL, de Kretser DM, Clarke IJ, Scheerlinck JP, Phillips DJ (2004) *J Endocrinol* 182:69–80.
- Matzuk MM, Kumar TR, Vassili A, Bickenbach RR, Roop DR, Jaenisch R, Bradley A (1995) *Nature* 374:354–356.
- Matzuk MM, Finegold MJ, Mather JP, Krummen L, Lu L, Bradley A (1994) *Proc Natl Acad Sci USA* 91:8817–8821.
- Matzuk MM, Finegold MJ, Su JJ, Hsueh AJW, Bradley A (1992) *Nature* 360:313–319.
- Gonzalez-Cadavid NF, Bhasin S (2004) *Curr Opin Clin Nutr Metab Care* 7:451–457.
- Lee SJ (2004) *Annu Rev Cell Dev Biol* 20:61–86.
- Schuelke M, Wagner KR, Stolz LE, Hubner C, Riebel T, Komen W, Braun T, Tobin JF, Lee SJ (2004) *N Engl J Med* 350:2662–2668.
- Reiz-Pousazas S, Bhasin S, Artaza JV, Shen R, Sinha-Hikim I, Hogue A, Fielder TJ, Gonzalez-Cadavid NF (2003) *Am J Physiol* 285:E876–E888.
- Zimmers TA, Davies MV, Koniaris LG, Haynes P, Esquela AF, Tomkinson KN, McPherron AC, Wolfman NM, Lee SJ (2002) *Science* 296:1486–1488.
- Sidis Y, Mukherjee A, Keutmann H, Delbaere A, Sadatsuki M, Schneyer A (2006) *Endocrinology* 147:3586–3597.
- Schneyer A, Sidis Y, Xia Y, Saito S, Re EE, Lin HY, Keutmann H (2004) *Mol Cell Biol* 24:25–28.
- Tortorello DV, Sidis Y, Holtzman DA, Holmes WE, Schneyer AL (2001) *Endocrinology* 142:3426–3434.
- Schneyer AL, Wang Q, Sidis Y, Sluss PM (2004) *J Clin Endocrinol Metab* 89:5067–5075.
- Hill JJ, Davies MV, Pearson AA, Wang JH, Hewick RM, Wolfman NM, Qiu Y (2002) *J Biol Chem* 277:40735–40741.
- Matzuk MM, Lu N, Vogel HJ, Sellheyer K, Roop DR, Bradley A (1995) *Nature* 374:360–363.
- Jorge CJ, Kysik M, Jamin SP, Behringer RR, Matzuk MM (2003) *J Mol Endocrinol* 18:953–967.
- Florio P, Luisi S, Marchetti P, Lupi R, Cobellis L, Falaschi C, Sugino H, Navalesi R, Genazzani AR, Petraglia F (2000) *J Endocrinol Invest* 23:231–234.
- Yamaoka T, Idegawa C, Yano M, Matsushima T, Yamada T, Ii S, Moritani M, Hata J, Sugino H, Noji S, et al. (1998) *J Clin Invest* 102:294–301.
- Brun T, Franklin I, St-Onge L, Bussan-Laubert A, Schoenle EJ, Wollheim CB, Gauthier BR (2004) *J Cell Biol* 167:1123–1135.
- Michael MD, Kulkarni RN, Postic C, Previs SF, Shulman GI, Magnuson MA, Kahn CR (2000) *Mol Cell* 6:87–97.
- Ho J, de Guise C, Kim C, Lemay S, Wang XF, Lebrun JJ (2004) *Cell Signal* 16:693–701.
- Brown CW, Li L, Houston-Hawkins DE, Matzuk MM (2003) *Mol Endocrinol* 17:2404–2417.
- Dufour DR, Lott JA, Nolte FS, Gretsch DR, Koff RS, Seeff LB (2000) *Clin Chem* 46:2050–2068.
- Osawa K, Abe K, Kurosawa N, Kurohmaru M, Sugino H, Takahashi M, Hayashi Y (1993) *FEBS Lett* 319:217–220.
- Wada M, Shintani Y, Kosaka M, Sano T, Hizawa K, Saito S (1996) *Endocr J* 43:375–385.
- Verspohl EJ, Ammon HP, Wahl MA (1993) *Life Sci* 53:1069–1078.
- Shiozaki S, Tajima T, Zhang YQ, Furukawa M, Nakazato Y, Kojima I (1999) *Biochim Biophys Acta* 1450:1–11.
- Prentki M, Nolan CJ (2006) *J Clin Invest* 116:1802–1812.
- Dor Y, Brown J, Martinez OI, Melton DA (2004) *Nature* 429:41–46.
- Bonner-Weir S, Weir GC (2005) *Nat Biotechnol* 23:857–861.
- Ogata T, Park KY, Seno M, Kojima I (2004) *Endocr J* 51:381–386.
- Weichenberg BL (2000) *Endocr Rev* 21:697–738.
- Barthel A, Schmol D (2003) *Am J Physiol* 285:E685–E692.
- Xia Y, Sidis Y, Schneyer A (2004) *Mol Endocrinol* 18:979–994.
- Boyantovsky BB, van der Westhuyzen DR, Webb NR (2005) *J Biol Chem* 280:32746–32752.